

FLUID: A rocket-borne pathfinder instrument for high efficiency UV band selection imaging

Nicholas Nell^{a,*}, Nicholas Kruczek^a, Kevin France^a, Stefan Ulrich^a, Patrick Behr^a, Emily Farr^a

^aLaboratory for Atmospheric and Space Physics, 1234 Innovation Drive, Boulder, CO, USA

Abstract. The Far- and Lyman-Ultraviolet Imaging Demonstrator (FLUID) is a rocket-borne arcsecond-level ultraviolet (UV) imaging instrument covering four bands between 92 – 193 nm. FLUID will observe nearby galaxies to find and characterize the most massive stars that are the primary drivers of the chemical and dynamical evolution of galaxies, and the co-evolution of the surrounding galactic environment. The FLUID short wave channel is designed to suppress efficiency at Lyman- α (121.6 nm), while enhancing the reflectivity of shorter wavelengths. Utilizing this technology, FLUID will take the first ever images of local galaxies isolated in the Lyman ultraviolet (90 – 120 nm). As a pathfinder instrument, FLUID will employ and increase the TRL of band-selecting UV coatings, and solar-blind UV detector technologies including microchannel plate and solid state detectors; technologies prioritized in the 2022 NASA Astrophysical Biennial Technology Report. These technologies enable high throughput and high sensitivity observations in the four co-aligned UV imaging bands that make up the FLUID instrument. We present the design of FLUID, status on the technology development, and results from initial assembly and calibration of the FLUID instrument.

Keywords: ultraviolet, multilayer coatings, telescope.

*Nicholas Nell, nicholas.nell@lasp.colorado.edu

1 INTRODUCTION

FLUID is a proposed rocket-borne arcsecond-level, multi-band imaging system operating across the Far UV (FUV; 120 – 200 nm) and Lyman UV (LUV; 90 – 120 nm) bands (see Figure 1), designed to investigate massive-star formation in nearby galaxies and obtain the first morphological classification of nearby galaxies in the LUV.¹ The highest mass stars (O- and B-type stars; $\approx 5 - 200 M_{\text{solar}}$ ²), born in short-lived bursts of star formation, dominate the stellar luminosity of these early galaxies and are the strongest drivers of a galaxy’s on-going kinematic and chemical evolution.³⁻⁵ The FLUID instrument will leverage a novel selection of channels to image local galaxies across the LUV and FUV bandpasses for the first time. The four channels selected for FLUID offer an observational handle to concurrently and consistently solve for the stellar temperature and dust extinction on spatial scales comparable to the size of star forming regions in those galaxies (~ 100 pc), an observation which is not possible using current orbital assets without costly spectroscopic observations of every cluster. These data, combined with archival observations, enable us to quantify the influence of O stars on the mass-chemical-energy cycle of the target galaxies. FLUID spatial resolution on local galaxies was further designed to match the resolution that JWST is currently achieving on high- z galaxies. Through the use of morphological classification, FLUID observations will be used in conjunction with JWST observations to track the spatial distribution of massive stars across cosmic time. The science traceability matrix (Figure 2) is used to inform and direct the instrument design and technology development discussed in the following sections. Currently, funding has been obtained to fabricate two channels of FLUID, F110M and F140M, which are actively being built and characterized.

2 INSTRUMENT DESIGN

2.1 Instrument Overview

The FLUID optical assembly comprises an array of four imaging channels, housed within a standard NASA Wallops Flight Facility (WFF) 22” diameter rocket skin (Figure 3). Each telescope module includes a 150 mm diameter $f/28.7$ Cassegrain telescope feeding either a CCD or microchannel plate (MCP) detector, depending on the channel (see Figure 3 and Table 1). The detector-area limited field-of-view has a $20'$ diameter. The telescope optics for F110M and F140M were fabricated by a division of Coherent (formerly Precision Asphere) with polishing capabilities, such as low microroughness and mid-spatial frequency control and metrology, demonstrated on UV optics.⁶ Two sets of telescope optics were acquired with the current funding and the remaining two sets will be purchased pending future proposal selection. Filters for the FLUID instrument are all reflective in nature and consist of multilayer coatings applied to the telescope optics optimized for high reflectivity of in-band light and low reflectivity of out-of-band light. The FLUID flight filters are defined by the primary and secondary telescope mirrors, each coated with a multilayer prescription specific to their designated bandpass (Section 3). The two-bounce reflection filter improves the out-of-band rejection, matching the configuration of *LUVVOIR/LUMOS*,⁷ an instrument which serves as a design prototype for a UV imaging and spectroscopy instrument for the upcoming *Habitable Worlds Observatory*. The LUMOS design utilizes 150 mm

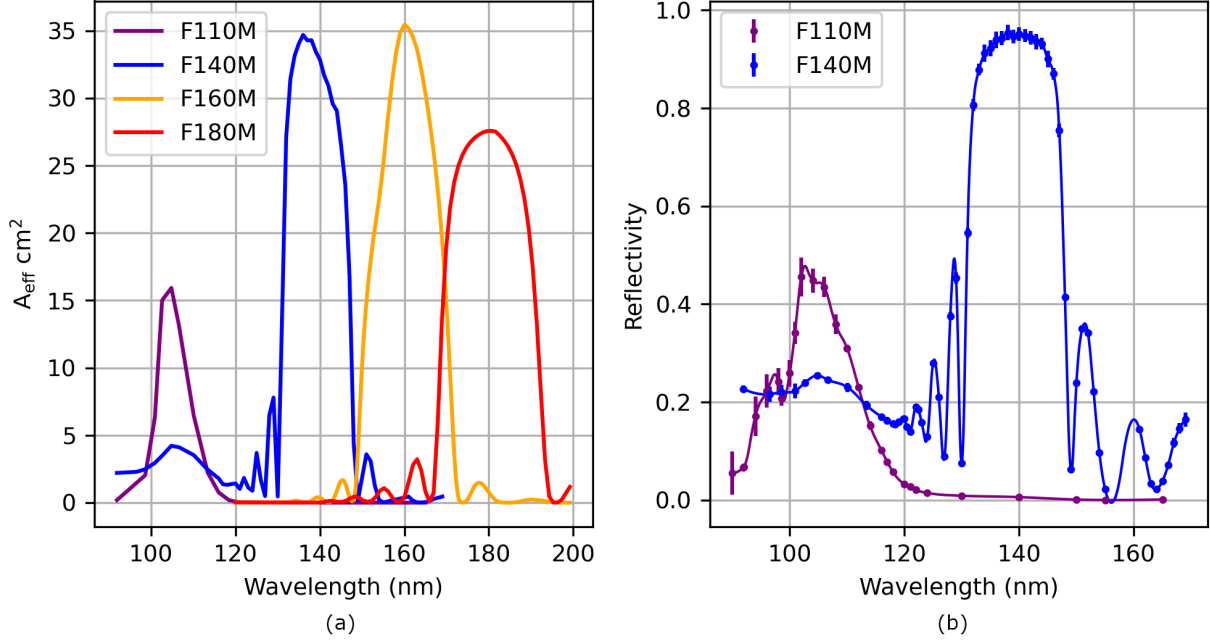


Fig 1: (a) Predicted effective area for each channel of FLUID based on empirical and theoretical coating efficiencies. F110M and F140M are based off of empirical reflectivity measurements of coated optics, F160M and F180M are based off of theoretical coating efficiencies. (b) Empirical measurements performed at LASP of primary mirrors for the F110M and F140M channels (see Section 3.1).

diameter shaped fold mirrors, the same size as the FLUID primary mirrors. The FLUID primary mirrors therefore provide an excellent prototype for TRL demonstration. A summary of the instrument optical specifications and effective areas (A_{eff}) can be found in Figure 1 and Table 1. Effective areas for F110M and F140M are created using measured reflectivities of the flight optics and predicted efficiencies of the detectors. Effective areas for F160M and F180M are created using theoretical coating efficiencies and predicted detector efficiencies.

Each FLUID channel will employ its own bandpass-optimized detector. The F110M and F140M channel detectors are 25 mm active diameter open-face cross-delay line (XDL) MCP detectors with opaque CsI photocathodes applied. The F140M, F160M, and F180M filters maintain low efficiency ($\sim 5\%$) at visible wavelengths allowing us to utilize detector technologies optimized for a specific UV bandpass without concern for significant contamination from visible wavelengths. The F110M filter is reflective at visible wavelengths, but the photocathode used for this channel, CsI, is not responsive at these wavelengths.^{9,10} F180M will utilize a 50 mm square sealed tube MCP¹¹ with a semi-transparent bialkali photocathode. Not only does this photocathode selection maximize the efficiency for FLUID science measurements in each bandpass, it is also the configuration baselined for *LUVUOIR/LUMOS*.⁷

FLUID will employ a CCD detector to maximize the throughput of the F160M channel (e.g., a passivated CCD¹²). Characterization results have been published for both surface passivation and anti-reflection (AR) coatings available from Teledyne e2v that substantially improve quantum efficiency (QE) in the FUV bandpass.^{13,14} The initial flight of FLUID will have a 27.6 mm square CCD42-40 with enhanced passivation and the “VUV1” AR coating from Teledyne e2v serve as the detector for the F160M channel. The CCD42-40 was chosen for its compatibility with the FLUID design and extensive space flight heritage.¹⁵⁻¹⁸ LASP has heritage with readout electronics for a CCD closely related to the CCD42-40 that are successfully operating on-orbit on the NASA *CUTE* mission.¹⁹

Alongside the assembly of the CCD, we will collaborate with JPL to develop a solar-blind AR coating for application to the CCD²⁰ to reject sensitivity across the visible bandpass. This coating will be applied to another CCD42-40 with enhanced passivation from Teledyne e2v, and this CCD will be integrated into the F160M channel prior to a planned second flight of FLUID. Performing this technology development on a device that already has high TRL provides an expedited path for its use on larger class missions with high reliability requirements.

Multi-band imaging is used in other fields as well and the FLUID instrument concept leverages aspects of the SDO-AIA design.²¹ Typically primary mirrors for astrophysical missions are larger due to the desire to maximize signal-to-noise ratios (SNR) for observations of faint targets. The multilayer coating process used for the FLUID optics is

NASA Science Goal	FLUID Science Objectives	Physical Parameters	Observable	FLUID Measurement Requirements			Mission Requirements											
				Parameter	Requirement	Projected												
<p>Understand how Stellar Feedback Drives the Evolution of Cosmic Ecosystems (Astro 2020, Sections 1.1,3, 2.3)</p>	<p>Measure the location and environmental impact of O stars, quantify their influence on wavelength-dependent galaxy morphology, and</p>	<p>1) LUV and FUV Luminosity of OB star populations and 2) Spatial distribution of OB star clusters</p>	<p>(Physical Parameter 1) LUV and FUV brightness distribution of FLUID target galaxies</p>	<p>Sensitivity</p> <p>S/N ≥ 7 per detector resolution element (≤ 100 pc spatial scale) in four FLUID bands for source fluxes $\geq 3.7 \times 10^{44}$ erg/cm²/s/A in a 300s exposure</p>	<p>Galaxy-integrated S/N > 30 in four FLUID bands for wavelength-dependent morphological classification.</p>	<p>S/N projections on faintest FLUID target: F110M = 75.0 F140M = 78.3 F160M = 174.1 F180M = 85.3</p>	<p>Telescope aperture, mirror surface quality, dielectric multi-layer coating reflectivity, detector DQE, 22" diameter rocket fanning</p>											
								<p>Dynamic Range</p>	<p>F = 8.3×10^{44} - 1.7×10^{45} erg/cm²/s/A at 1400 Ang. per 100 pc spatial scale</p>	<p>F = 1.9×10^{44} - 1.0×10^{45} erg/cm²/s/A at 1400 Ang. per 100 pc spatial scale (S/N = 1 limit in faintest galaxy cluster to the detector 5% non-linearity limit)</p>	<p>Low noise UV detector, launch window within +/- 1.5 hours of local midnight to minimize airglow background</p>							
												<p>Total Bandwidth</p>	<p>Four channels covering the LUV and FUV bandpasses</p>	<p>919 - 1933 Ang</p>	<p>Space platform because no atmospheric transmission at these wavelengths, bandpass-selecting di-electric multi layer coatings</p>			
																<p>Channel Spectral Resolution</p>	<p>Resolving Power = $\lambda/\Delta\lambda > 4$, where $\Delta\lambda$ is defined at the 95% integrated filter bandpass</p>	<p>F110M ($\Delta\lambda = 919 - 1144$ Ang, $\lambda/\Delta\lambda = 4.7$) F140M ($\Delta\lambda = 1254 - 1499$ Ang, $\lambda/\Delta\lambda = 5.6$) F160M ($\Delta\lambda = 1484 - 1718$ Ang, $\lambda/\Delta\lambda = 6.8$) F180M ($\Delta\lambda = 1679 - 1933$ Ang, $\lambda/\Delta\lambda = 7.1$)</p>
<p>Angular Resolution</p>	<p>5-4.2 arcsec (corresponds to 100 pc at the most distant FLUID target galaxy)</p>	<p>2.2 arcsec (combining detector resolution, telescope PSF, and rocket ACS)</p>	<p>Telescope figure and optomechanical alignment, 1-arcsecond attitude control system</p>															
<p>Instantaneous FOV</p>	<p>≥ 10 arcmin to capture extent of galactic UV emission morphology</p>	<p>20 arcmin</p>	<p>Optical system plate scale</p>															
	<p>(Physical Parameter 2) Angular Distribution of OB clusters at projected spatial scale of ≤ 100 pc</p>		<p>(Physical Parameter 1) LUV and FUV colors of OB star clusters</p>															
	<p>(Physical Parameter 2) Concentration, Asymmetry, and Clumpiness (CAS) parameters of OB star populations</p>																	

Fig 2: FLUID science traceability matrix.

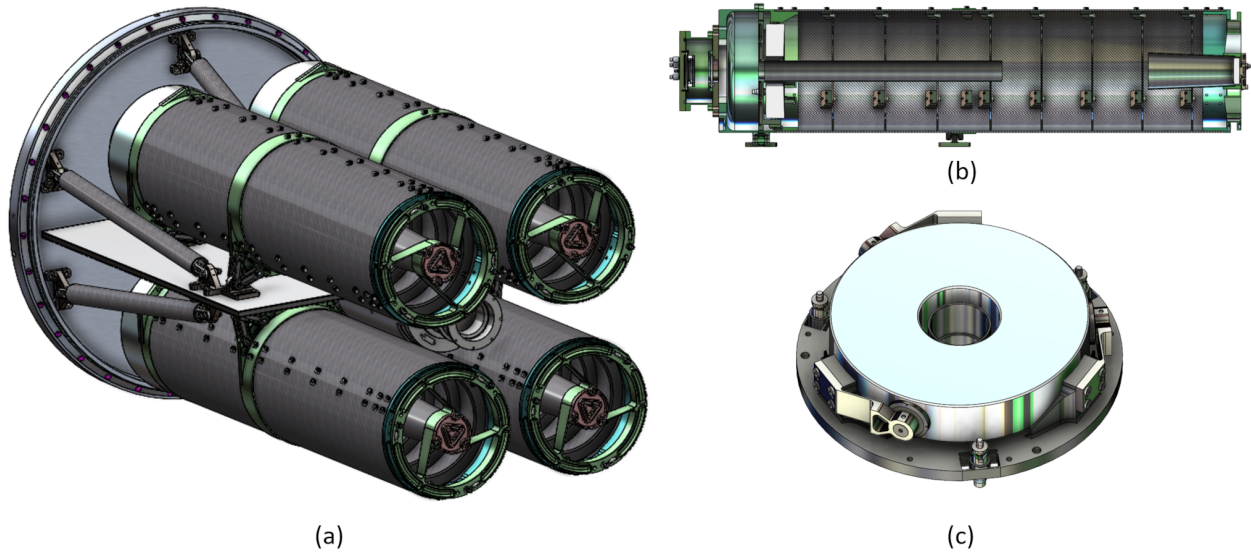


Fig 3: (a) A CAD rendering of the full FLUID instrument. The four telescope modules are mounted to a hermetic, 22" bulkhead, and arranged about the roll axis of the rocket. The NASA-provided ST5K star tracker⁸ is shown at the center of the telescope array. (b) A cutaway view of a single FLUID telescope. (c) A CAD rendering of the primary mirror mount.

currently limited to ~ 150 mm in diameter due to mechanical limitations of the coating chamber. The sounding rocket envelope limits the largest possible optic diameter to ~ 500 mm. While it is possible to build a large single telescope with four integrated reflective filter imaging channels, there are a variety of complications that make this concept less desirable than independent optical channels. The additional optics required to split and reimage the field after filtering add efficiency losses and the system would be more complicated to align and characterize. The independent channel design allow each channel to be assembled, aligned, and characterized independently and each channel has a mounting system with adjustment to allow for coalignment of all the channels when they are mounted to the sounding rocket optical bench (See Figures 4 and 3).

2.2 Optical Mounts

The optical mount for the primary mirror is based on the design of the Interface Region Imaging Spectrograph (IRIS) primary mirror mount,^{22,23} a design also adopted on the Hi-C sounding rocket mission.²⁴ The flexures and bond pads have been modified for the FLUID primary mirrors based on anticipated launch loads and historical data from previous sounding rocket missions. The use of tangential flexures minimizes the diameter of the cell to allow all four channels to fit within the sounding rocket envelope. We have also employed a cell with Maxwell kinematic coupling points²⁵ to attach the primary mirror cell to the optical metering tube assembly. The primary mirror cell can be adjusted in tip and tilt to align the mirror on the optomechanical axis of the system. The FLUID secondary mirror is sufficiently small that it is possible to use a simpler "pedestal" style mount with a single bond on the back surface of the optic. The secondary mirror cell has integrated cutout style flexures to reduce the amount of stress on the optic. Tip, tilt, and piston adjustment of the secondary mirror is accomplished by moving the secondary spider structure which is also mounted to the optical metering tube using a Maxwell kinematic coupling. Once optimal alignment is achieved, the three mount points are measured and the mounting hardware is trimmed to set the desired distances. Fine adjustments are made with shims if necessary. This method is used to ensure minimal possible movement or settling under the strenuous vibration environment of sounding rocket flights.

2.3 Instrument Resolution

Final instrument imaging resolution is driven by three major components: the telescope PSF, the detector response function, and the attitude control system (ACS) jitter. The final observed resolution in the instrument is the convolution of each of these components.²⁶ The observation-driven specification for the resolution of each channel is a PSF with $4.2''$ full width at half maximum (FWHM). The $4.2''$ angular resolution requirement corresponds to a spatial scale of 100 pc for the furthest FLUID target. This spatial scale is selected to be compatible with high-redshift scales

Table 1: FLUID Instrument Summary

Instrument Parameters	
Number of Channels	4
Focal Ratio	$f/28.7$
Bandpass	91.9 – 193.3 nm
Field of View	20' diameter
Instrument Plate Scale	48'' mm ⁻¹
Instrument Peak A_{eff} (F110M)	16 cm ²
Instrument Peak A_{eff} (F140M)	35 cm ²
Instrument Peak A_{eff} (F160M)	35 cm ²
Instrument Peak A_{eff} (F180M)	28 cm ²
Effective Focal Length	4300.3 mm
Total Instrument Length	870 mm
Cassegrain Parameters	
Primary Diameter	150.0 mm
Primary Radius of Curvature	1800.0 mm
Secondary Diameter	42.0 mm
Secondary Radius of Curvature	459.8 mm
Detector Parameters	
Number of Detectors	4
F110M	CsI MCP
F140M	CsI MCP
F160M	Passivated CCD
F180M	Bialkali MCP tube

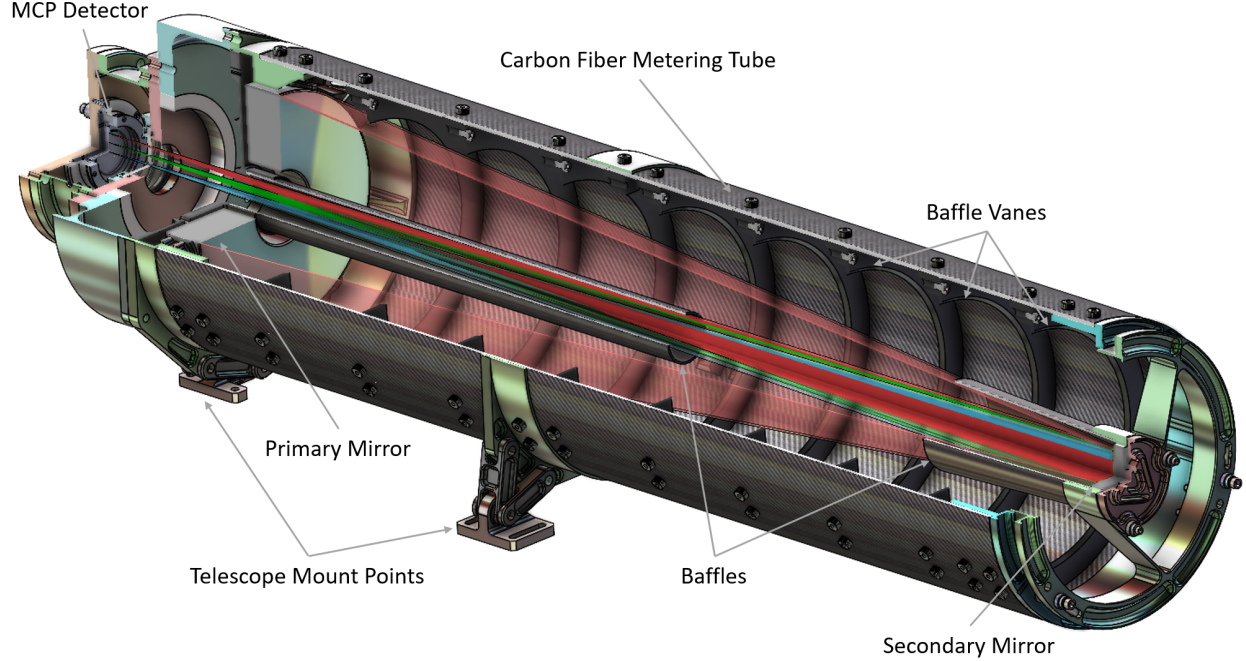


Fig 4: Cutaway CAD rendering of a single FLUID telescope. Light paths are shown in blue, green, and red corresponding to light falling on the center, midpoint, and edge of the detector respectively.

targeted by future large UVOIR missions²⁷ and to enable comparison with high-redshift images obtained by JWST.²⁸ The component and total resolution estimates are shown in Table 2. Currently we estimate a telescope PSF of 1.2'' FWHM through analysis using Zemax OpticStudio software based on fabrication tolerances and expected mechanical

alignment tolerances. Due to the nature of the position detection in XDL and XS anode MCP readouts, rather than attempting to quantify the response function as the size of a pixel it is advantageous to instead describe the position as a “resolution element” (resol) since there are no physical pixels in the MCP readout.^{29,30} The resolution element describes the limiting imaging performance of the MCP detector as a system incorporating all elements in the MCP detector that can affect imaging resolution. Each type of detector has a different response function. The XDL MCP detectors for F110M and F140M have specifications of 30 μm FWHM resols. The F180M XS MCP detector has a specification of 20 μm FWHM resols. The CCD42-40 has 13.5 μm square pixels. These resols can be described with a Gaussian shape and thus we use a single number such as the FWHM of the resol to describe the response function of XDL and XS anode MCP readouts. Finally, the jitter of the ACS during observations must also be considered. Using vehicle performance reports from past sounding rocket flights we estimate a predicted ACS jitter FWHM of $< 0.5''$. Each of these components is mapped to angular space in Table 2 using the instrument plate scale (see Table 1) to directly compare and convolve magnitudes of the different components. Ultimately, after considering all contributions to the final resolution of FLUID, we predict that all channels fall within the specification of $4.2''$ FWHM with $> 100\%$ margin.

Table 2: FLUID In-band Resolution Budget

Channel	Telescope	Detector	ACS	Total (FWHM)	Margin ^a
F110M	$0.8''^{\text{b}}$	$1.4''$	$0.5''$	$\leq 2.0''$	110%
F140M	$1.2''^{\text{c}}$	$1.4''$	$0.5''$	$1.9''$	121%
F160M	$1.2''^{\text{c}}$	$0.7''$	$0.5''$	$1.4''$	200%
F180M	$1.2''^{\text{c}}$	$1.0''$	$0.5''$	$1.6''$	162%

^a Note: the FLUID PSF requirement is $4.2''$ FWHM.

^b Empirically characterized upper limit at visible wavelengths.

^c Predicted performance.

2.4 Optomechanical Structural Analysis

Structural analysis was performed on the primary mirror assembly to verify that the design would survive the sounding rocket vibration environment. A finite element model was constructed with Ansys to analyze the primary mirror assembly. Static analysis with torque values to be used for flight shows that the primary mirror surface deforms less than 1.3 nm peak-to-valley, shown in Figure 5, which is well within the figure specification (See Figure 7) required to achieve the desired PSF. This model is used in conjunction with the vibration levels presented in Table 6.3.4-1 of the NASA Sounding Rockets User Handbook³¹ to analyze the primary mirror assembly. The first and second modes occur at 314.8 Hz and 366.6 Hz respectively and are shown in Figure 6. The first mode is primarily along the optical axis of the system and the second mode is mainly lateral. These are the most notable modes and analysis shows that the primary mirror assembly will handle the vibration environment with substantial margin. Both static and vibration analysis show that each component in the primary mirror assembly exceeds the factor of safety outlined in the NASA structural design standard document NASA-STD-5001A. A full thermal analysis has not yet been performed but past data demonstrate that the temperature range experienced by the telescopes in flight will be small due to the isolation from the aluminum structure provided by the carbon fiber optical metering tubes. The thermal effect on the optical metering tube is minimal and well within the tolerances of the optical system. The thermal isolation provided by the optical metering tube allows a stable thermal operating environment for the optics and optical mounts.

3 TECHNOLOGY DEVELOPMENT

FLUID aims to accomplish development and maturation of several technologies critical for future missions. These technologies include FUV and LUV reflective bandpass filters on large substrates, sealed tube MCP detectors with bialkali photocathodes and cross strip (XS) anodes, passivated CCD detectors to improve QE at UV wavelengths, and solar-blind multilayer coatings for silicon detectors.

3.1 FUV Band-selecting Filters

FLUID bandpasses are defined by reflective multilayer coatings developed in collaboration with the Consejo Superior de Investigaciones Científicas (CSIC) Grupo de Óptica de Láminas Delgadas (GOLD)¹. NASA’s 2022 Astrophysics

¹<https://gold.io.csic.es/>

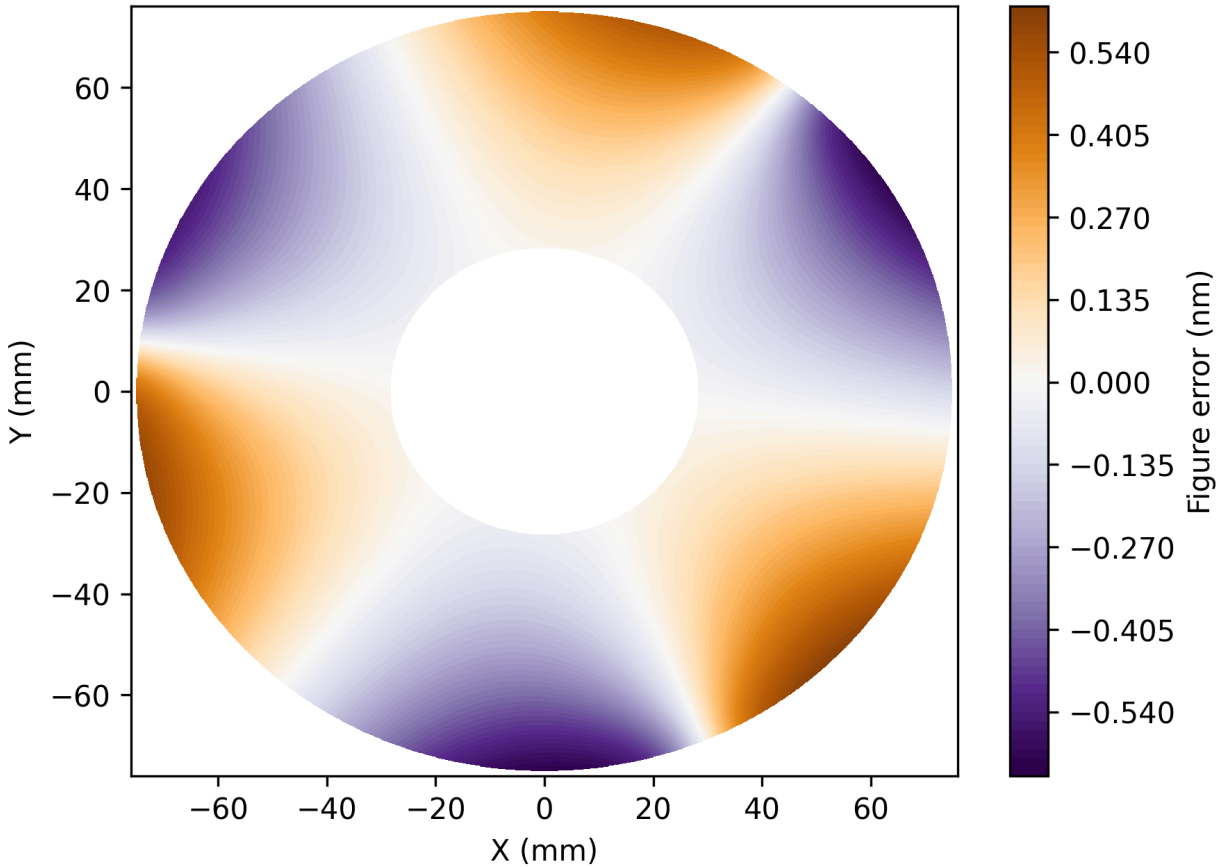


Fig 5: Finite element analysis prediction of primary mirror figure error induced from the mechanical mount. The peak-to-valley value is 1.24 nm with an RMS of 0.25 nm.

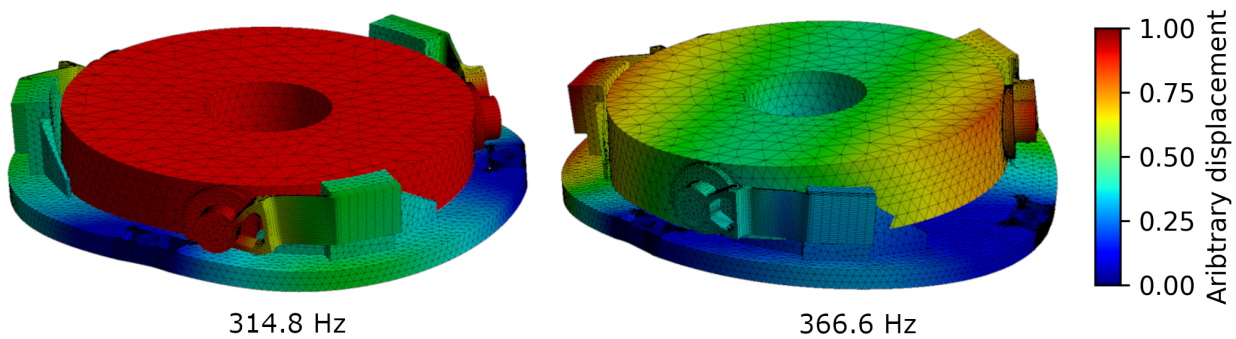


Fig 6: Results of modal analysis of the FLUID primary mirror assembly. The first mode occurs at 314.8 Hz (left) and the second mode occurs at 366.6 Hz (right). Displacements generated by modal analysis (shown in the colormap) are qualitative and are thus shown on an arbitrary scale.

Biennial Technology Report lists “High-Throughput Bandpass Selection for UV” and “Far-UV Imaging Bandpass Filters” as Tier 1 and Tier 3 technologies, respectively, to be developed for future NASA missions.³² Initially, coating prescriptions are modeled to perform trade studies on total throughput, out-of-band rejection, and effective filter width. Once an optimal prescription is identified, test depositions are performed on 2” × 2” witness samples, which are measured across the bandpass of interest to verify performance. This process is repeated until the sample matches the modeled prescription to within typical deposition process, material, and modeling tolerances. Finally, each flight optic is coated in a separate run alongside a witness sample. Witness samples are measured on-site at a facility described in References 33 and 34 prior to shipment to LASP. Each witness sample and optic is then measured at LASP in

the “square tank” facility (See Figure 1) to verify performance of the flight optics versus their witness samples and quantify any changes that may have occurred during shipment.^{35,36} Flight optics are measured at multiple points across their clear aperture to quantify uniformity of the bandpass filter. After measurements the optics are stored in active nitrogen purge boxes and the witness samples are stored in controlled humidity chambers. Witness samples are then regularly measured to quantify degradation at different relative humidity levels. Details of this process and measurements of the coatings on flight optics are described in Reference 37.

3.2 Solar-blind FUV Detectors

NASA’s 2022 Astrophysical Biennial Technology Report also lists “Large-Format, Low-Darkrate, High-Efficiency, Photon-Counting, Solar-blind, Far- and Near-UV Detectors” as a Tier 1 priority.³² For the F180M channel, a sealed tube MCP detector with a semi-transparent bialkali photocathode and an XS anode has been baselined in collaboration with the Space Sciences Laboratory at UC Berkeley. This detector exploits the reliability of commercially available sealed tube technology (the Photonis Planacon) but substitutes the typical commercial anode, which is only capable of low resolution imaging, for an XS anode capable of high resolution imaging. The semi-transparent bialkali photocathode applied to the window of the sealed tube has a short wavelength cutoff of ~ 160 nm due to the transmissivity of the window material and will be optimized to reduce sensitivity at visible wavelengths.^{11,38} The MCPs in this detector will be processed via atomic layer deposition to tune the resistance and secondary emission characteristics. Ultimately, this results in an MCP detector with good gain and stability characteristics.^{39,40}

For the first planned flight of the FLUID F160M channel we have baselined a passivated CCD42-40 with an AR coating expected to achieve a quantum detection efficiency of 30 – 40% over the F160M bandpass.¹⁴ We will thoroughly characterize this device in the FUV at predicted flight operating temperatures. A benefit of the CCD42-40 is the ability to operate the device at Peltier temperatures such that temperatures under -40°C result in a system dominated by read noise. For characterization testing we typically achieve these temperatures using a thermoelectric cooler¹⁹ and for flight we will leverage a cooling design from the LASP SDO-EVE calibration sounding rocket.⁴¹ The unique facilities at LASP allow measurements of reflectivity of such a device to be made across the FUV bandpass. Facilities at LASP designed for detector characterization in the FUV also allow QE to be measured for the device and in-band flat fields to be generated.^{19,42} This suite of fundamental measurements enables calculations of quantum yield and charge collection efficiency to be made in the FUV bandpass to thoroughly characterize current performance capabilities.

In collaboration with JPL, we plan to coat a passivated CCD42-40 with a solar-blind metal-dielectric coating prescription ($\text{Al}/\text{Al}_2\text{O}_3$) that maintains good detector efficiency ($\sim 20\%$) in the F160M bandpass while holding sensitivity across the entire visible bandpass to a low level ($< 4\%$).²⁰ Despite a drop in in-band performance, it is the significant out-of-band suppression that is critical for improving SNR in FUV observations with a CCD. CCDs inherently have high QE (40 – 65%) across the full visible bandpass due to the optical properties of silicon. Reducing the out-of-band sensitivity by an order of magnitude significantly reduces background noise from sources such as scatter, other objects in the FOV, and out-of-band flux from target objects. This technology is vital for improving SNR across the FUV bandpass where silicon is inherently less sensitive. The coating performance will be characterized at LASP through measurements of reflectivity and QE across the FUV and visible bandpasses.

4 ASSEMBLY

The optical substrate material of the telescope optics is Schott N-BK7, which is chosen to reduce stress in the multi-layer coatings by attempting to thermally match to the fluoride materials used in the multilayer coating process.^{43,44} Metrology details for the F110M primary and secondary mirrors prior to coating are shown in Figure 7. The guideline power spectral density (PSD) shown in Figure 7 was designed to meet the projected final telescope PSF of $\leq 1.2''$ FWHM. The optical metering tube and associated baffle tubes were acquired from Ability Composites. Internal baffle tubes are bonded directly to the optical cells to be well coaligned with the optical path to avoid vignetting. The optical metering tube has been cleaned and vacuum baked to verify cleanliness and low outgassing prior to having baffle vanes installed (see Figure 9).

The F110M and F140M telescopes are currently being assembled and all telescope optics for F110M and F140M are coated, characterized, and in nitrogen purged storage at LASP. An image of the F110M primary mirror after being bonded to its cell is shown in Figure 8. Prior to assembly all optics were characterized in the LASP “square tank” facility and compared to their witness samples. Results from this calibration run and additional aging studies are discussed in detail in Reference 37. Bonding of the F110M secondary optic has been completed and final telescope

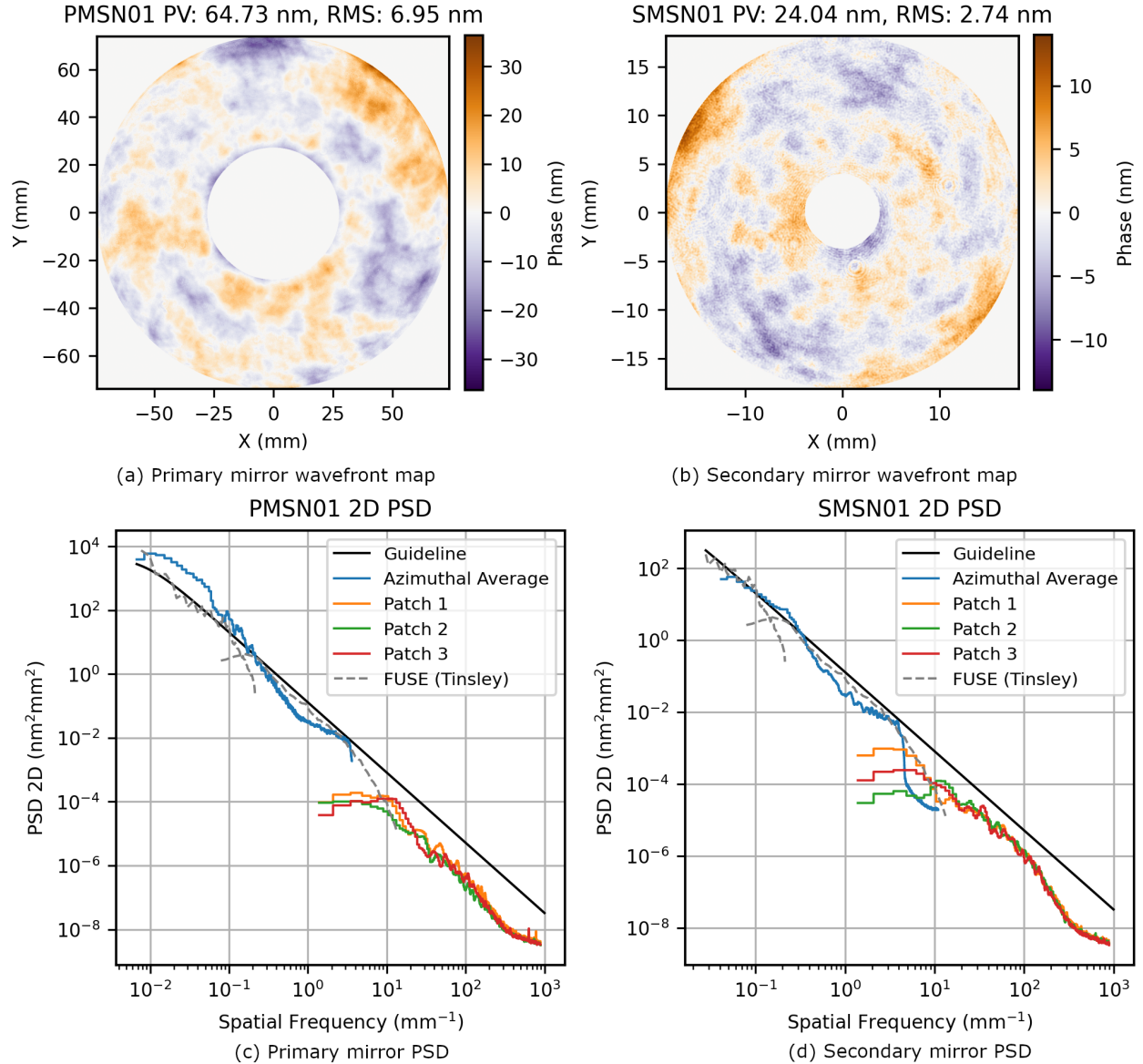


Fig 7: Metrology data for the FLUID F110M primary and secondary mirrors. Wavefront maps for each mirror are shown in panels (a) and (b). Power spectral density data is shown in panels (c) and (d). Blue lines show azimuthally averaged 2D PSD data for the FLUID F110M mirrors. PSD data for higher spatial frequencies is shown for a series of small patches (sized 0.36×0.27 mm). *FUSE* PSD data from Reference 45 is shown for comparison.

assembly and alignment occurred in September through November 2023. Following the buildup of F110M the same process will be repeated for F140M. The F110M and F140M MCP detectors are currently undergoing optimization at Sensor Sciences LLC and will be delivered in February 2024. The F110M detector assembly is shown in Figure 9.

5 TELESCOPE OPTICAL ALIGNMENT

5.1 Alignment Method

Telescope alignment is accomplished in two steps. First, the primary mirror cell is adjusted in tip/tilt to coalign the optical axis of the primary mirror with the optical metering tube. To do this, the telescope is mounted to an optical bench with the secondary mirror not installed, a bright point source that exits a pinhole is placed on the telescope optomechanical axis at a distance of the radius of curvature of the primary mirror. The primary mirror cell is adjusted in tip and tilt via shim under the kinematic mount points until the return point is coaligned with the exit pinhole of the

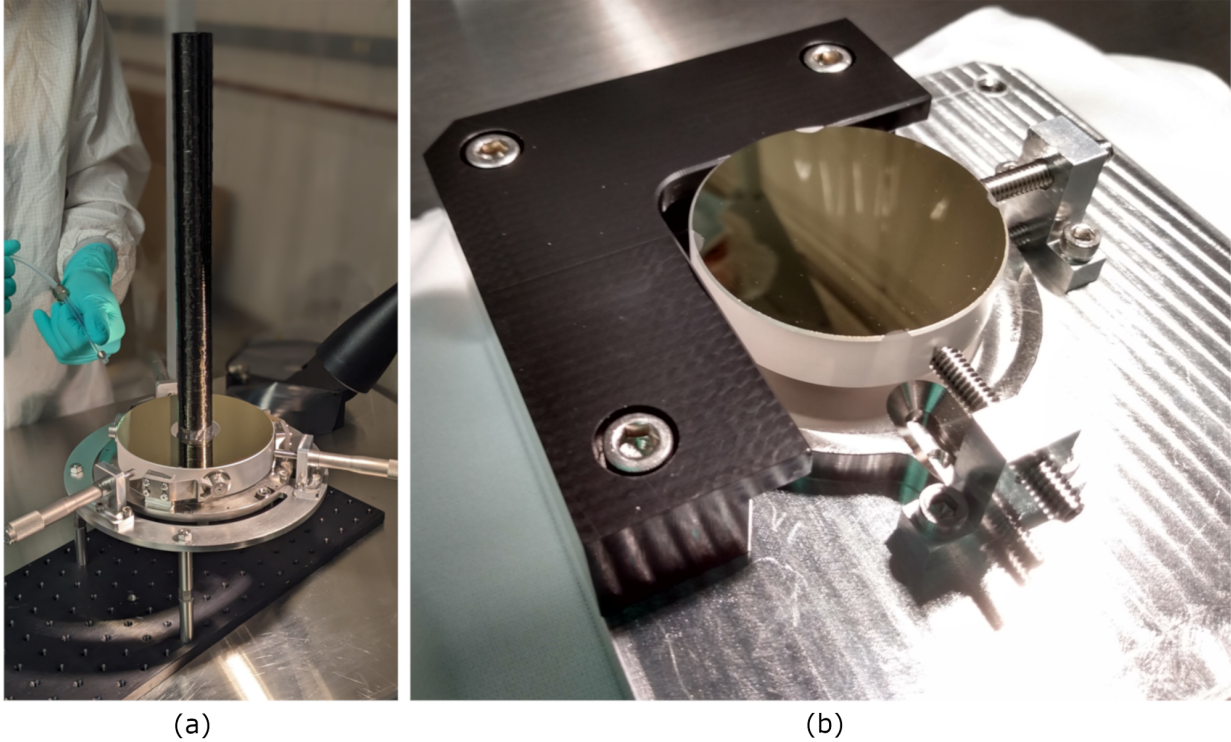


Fig 8: (a) The F110M primary mirror bonded in place to the optical cell including central baffle. (b) The FLUID F110M secondary mirror in its bonding fixture.

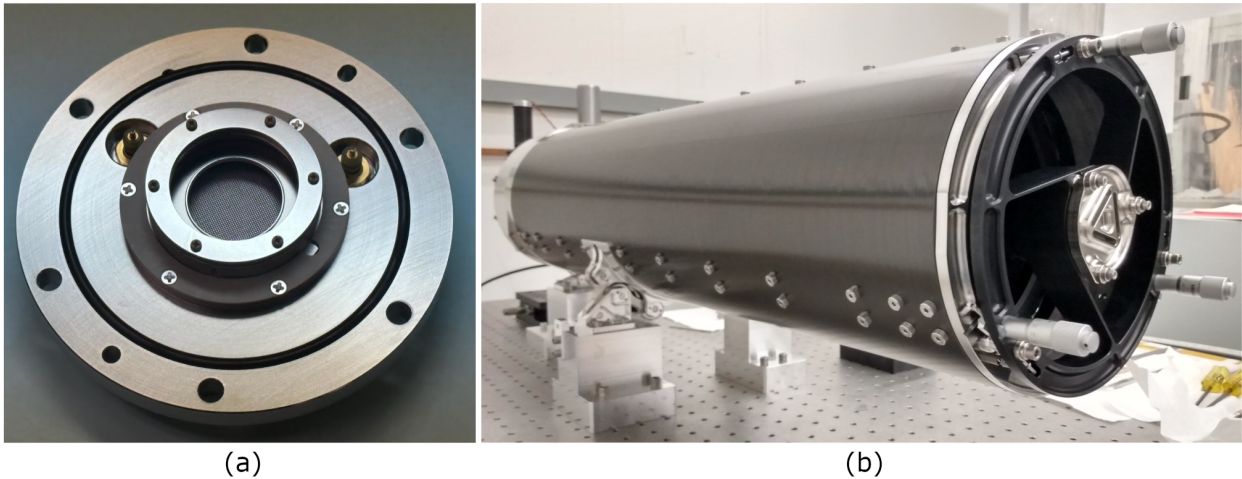


Fig 9: (a) A FLUID open face XDL MCP detector. (b) The FLUID F110M telescope in the optical alignment setup.

source. The primary cell is then locked in place and the secondary mirror is installed. A double pass system is used to align the secondary mirror of the telescope. A 10 inch flat mirror is placed away from the aperture and a point source microscope (PSM) is placed at the focal plane. The PSM is similar in design to those shown in References 46, 47, and 48 and was designed and built at LASP for optical alignments. The light source used in conjunction with the PSM has a wavelength of 530 nm and an adjustable source diameter. The secondary mirror is adjusted in tip, tilt, and piston until the return PSF observed in the PSM is symmetric with a profile that is consistent with optical modeling including fabrication and mounting tolerances of the system. Initially the secondary mirror is moved in tip, tilt, and piston with three micrometers. This allows verification of the telescope performance and in this state shim sizes for fixing the secondary mirror into place are estimated. Final secondary mirror adjustments are made by removing the micrometers and installing shims under the kinematic mount points to adjust the secondary mirror in tip, tilt, and piston. Secondary

mirror adjustments are decoupled to simplify the process, first, the tip and tilt are determined and those adjustments are made until the return spot is centered on the focal plane to within acceptable tolerance. Next, piston adjustments are made to focus the telescope onto the mechanical focal plane location. All optical mounts have been torqued into place using torque values suitable for flight. Final verification will be performed in-band in the LASP “longtank” facility. This facility is a large (30 inch inner diameter) vacuum chamber with a 24 inch Newtonian collimator illuminated with a flowing gas hollow cathode discharge lamp.⁴⁹

5.2 Alignment Results

The FLUID F110M telescope achieves nearly diffraction limited performance in the visible bandpass. The measured and predicted PSF are shown in Figure 10. It is critical to note that the PSF displayed in Figure 10 contains double the wavefront error of the telescope itself due to the nature of the light path in a double pass autocollimation test. However, because we do not currently have a method to measure the wavefront error of this system, it is not straightforward to remove excess contributions from the double pass test results. Therefore, this result overestimates aberration in the system. Additionally this telescope has been tested horizontally but is designed to operate in free fall during a sounding rocket flight. Finite element analysis of the gravity load on the primary mirror flexures shows that some astigmatism will be introduced to the primary mirror surface in the testing orientation under gravity load. The source used to illuminate the telescope for this alignment has a diameter of 10 μm and a “tophat” shape. Although the PSM is capable of producing smaller source diameters this size is used to provide sufficient intensity to produce a suitable SNR on the sensor. A source diameter of $\sim 3.2 \mu\text{m}$ or smaller would be required to properly resolve the PSF.⁵⁰ Additionally this PSF has been characterized with a 530 nm source but because the F110M central wavelength is 105 nm we expect the results from testing at 530 nm to scale with wavelength when F110M is illuminated with in-band light. Ultimately, considering all above contributions to the measured PSF, we expect the results shown in Figure 10 to be an upper limit estimate on the in-band performance of the F110M telescope. Figure 10 shows modeled contributions to the PSF from the detector resolution element and jitter of the ACS in flight. Additionally, the theoretical diffraction limited performance computed with the POPPY software⁵¹ is shown along with the detector and ACS convolved diffraction limited performance as a comparison against empirical F110M performance. With all contributions included we predict a PSF for F110M with an FWHM $\leq 2.0''$, resulting in a margin of 110% for the FLUID 4.2'' requirement.

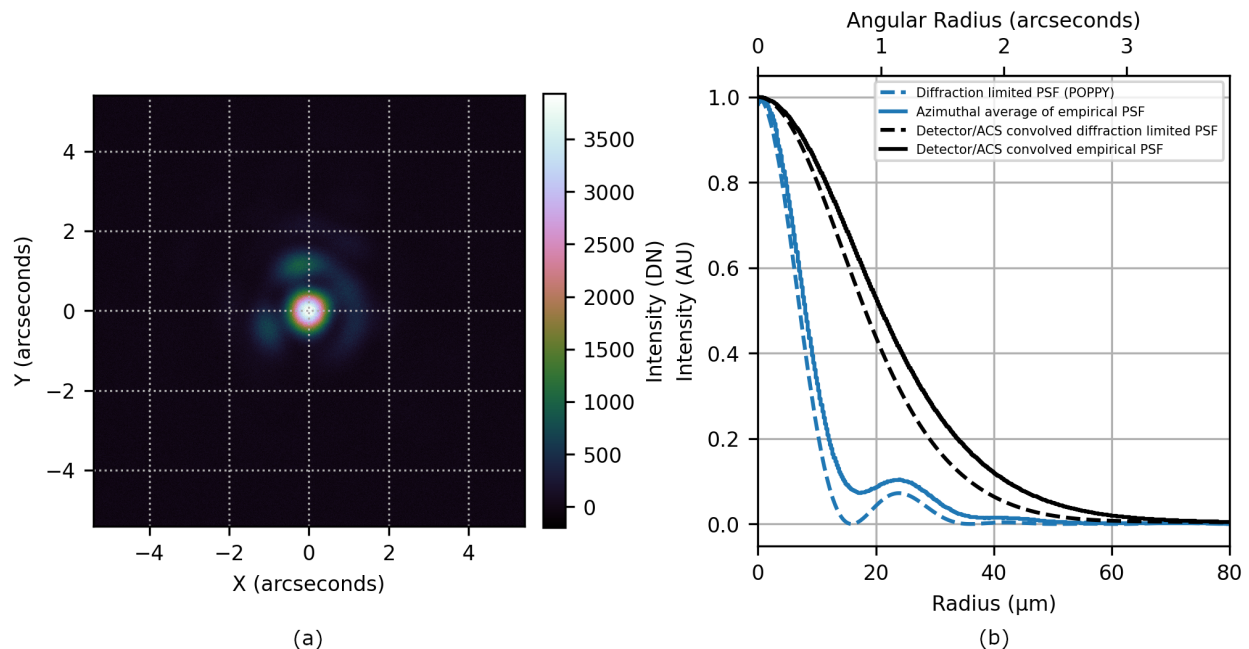


Fig 10: (a) shows the FLUID F110M PSF as observed with the PSM using 530 nm light. Diffraction features are clearly visible. Panel (b) shows the azimuthally averaged profile of the PSF shown in panel (a) along with the predicted performance after factoring in the detector resolution element and estimated ACS performance. For comparison we also show the theoretical diffraction limited performance.

6 SUMMARY

This paper has described the design and current state of the FLUID instrument, a four channel multi-band LUV and FUV imaging system. We have described the expected optical performance over the full bandpass of 92 – 193 nm and the technology required to achieve the desired performance in each channel. The executed and planned technology development of FUV multilayer coatings, sealed tube MCPs, passivated CCDs, and solar-blind CCD multilayer coatings are summarized and their important role in optimization of each of the FLUID channels is discussed. We have presented the current state of the FLUID F110M and F140M channels, which will continue to be assembled, tested, and characterized through the summer of 2024. The optical alignment results for F110M meet requirements with a significant margin and demonstrate a robust design that will be repeated for the remaining FLUID telescopes. The FLUID team is working hard to demonstrate the instrument capability with the funding available currently and will propose for funding through the 2023 ROSES/APRA call to complete the FLUID optical system development, advance the optical and sensor technology as described above, and realize the full potential of the FLUID concept with observations of several galaxies across three sounding rocket flights.

Code, Data, and Materials Availability

The data that support the findings of this paper are not publicly available. They can be requested from the author at nicholas.nell@lasp.colorado.edu.

Acknowledgments

The FLUID team would like to thank GOLD for their excellent coatings and great attention to detail throughout the process of developing, applying, and characterizing the multilayer coatings for FLUID. This research made use of POPPY, an open-source optical propagation Python package originally developed for the *James Webb Space Telescope* project.⁵¹ We thank Daniel Warren of CIRES for efforts on fabricating optical mounting hardware. This work was supported by NASA grant 80NSSC21K2016 to the University of Colorado.

References

- 1 N. Nell, N. Kruczek, K. France, *et al.*, “FLUID: a rocket-borne pathfinder instrument for high efficiency UV band selection imaging,” in *UV, X-Ray, and Gamma-Ray Space Instrumentation for Astronomy XXIII*, O. H. Siegmund and K. Hoadley, Eds., **12678**, 1267807, International Society for Optics and Photonics, SPIE (2023).
- 2 P. A. Crowther, O. Schnurr, R. Hirschi, *et al.*, “The R136 star cluster hosts several stars whose individual masses greatly exceed the accepted $150M_{\text{solar}}$ stellar mass limit,” *MNRAS* **408**, 731–751 (2010).
- 3 J. P. Grimes, T. Heckman, A. Aloisi, *et al.*, “Observations of Starburst Galaxies With Far-Ultraviolet Spectrographic Explorer: Galactic Feedback in the Local Universe,” *ApJS* **181**, 272–320 (2009).
- 4 C. Kobayashi and N. Nakasato, “Chemodynamical Simulations of the Milky Way Galaxy,” *ApJ* **729**, 16 (2011).
- 5 N. Langer, “Presupernova Evolution of Massive Single and Binary Stars,” *ARA&A* **50**, 107–164 (2012).
- 6 J. Kong and K. Young, “Ultra-smooth finishing of aspheric surfaces using CAST technology,” *Advanced Optical Technologies* **3**, 279–291 (2014).
- 7 K. France, B. Fleming, G. West, *et al.*, “The LUVOIR Ultraviolet Multi-Object Spectrograph (LUMOS): instrument definition and design,” in *Society of Photo-Optical Instrumentation Engineers (SPIE) Conference Series*, O. H. Siegmund, Ed., *Society of Photo-Optical Instrumentation Engineers (SPIE) Conference Series* **10397**, 1039713 (2017).
- 8 J. W. Percival, K. H. Nordsieck, and K. P. Jaehnig, “The ST5000: a high-precision star tracker and attitude determination system,” in *Space Telescopes and Instrumentation 2008: Optical, Infrared, and Millimeter*, J. Oschmann, Jacobus M., M. W. M. de Graauw, and H. A. MacEwen, Eds., *Society of Photo-Optical Instrumentation Engineers (SPIE) Conference Series* **7010**, 70104H (2008).
- 9 L. V. R. D. Marcos, J. I. Larruquert, J. A. Méndez, *et al.*, “Lyman- β ; narrowband coatings with strong lyman- α ; rejection,” *Opt. Express* **26**, 25166–25177 (2018).
- 10 A. Tremsin and O. Siegmund, “Uv radiation resistance and solar blindness of csi and kbr photocathodes,” *IEEE Transactions on Nuclear Science* **48**(3), 421–425 (2001).
- 11 O. H. W. Siegmund, T. L. Curtis, J. B. McPhate, *et al.*, “High performance cross strip imaging readout Planacon sealed tubes,” *Nuclear Instruments and Methods in Physics Research A* **1049**, 168077 (2023).

- 12 R. A. Stern, L. Shing, and M. M. Blouke, “Quantum efficiency measurements and modeling of ion-implanted, laser annealed chage-coupled and optical data,” *Appl. Opt.* **33**, 2521 (1994).
- 13 J. Heymes, M. Soman, G. Randall, *et al.*, “Comparison of Back-Thinned Detector Ultraviolet Quantum Efficiency for Two Commercially Available Passivation Treatments,” *IEEE Transactions on Nuclear Science* **67**, 1962–1967 (2020).
- 14 J. Heymes, M. Soman, T. Buggey, *et al.*, “Calibrating Teledyne-e2v’s ultraviolet image sensor quantum efficiency processes,” in *Society of Photo-Optical Instrumentation Engineers (SPIE) Conference Series, Society of Photo-Optical Instrumentation Engineers (SPIE) Conference Series* **11454**, 114541G (2020).
- 15 R. A. Howard, J. D. Moses, A. Vourlidas, *et al.*, “Sun Earth Connection Coronal and Heliospheric Investigation (SECCHI),” *Space Sci. Rev.* **136**, 67–115 (2008).
- 16 C. J. Eyles, R. A. Harrison, C. J. Davis, *et al.*, “The Heliospheric Imagers Onboard the STEREO Mission,” *Sol. Phys.* **254**, 387–445 (2009).
- 17 R. Kano, T. Sakao, H. Hara, *et al.*, “The Hinode X-Ray Telescope (XRT): Camera Design, Performance and Operations,” *Sol. Phys.* **249**, 263–279 (2008).
- 18 H. U. Keller, C. Barbieri, P. Lamy, *et al.*, “OSIRIS The Scientific Camera System Onboard Rosetta,” *Space Sci. Rev.* **128**, 433–506 (2007).
- 19 N. Nell, N. DeCicco, S. Ulrich, *et al.*, “Development and characterization of the CCD detector for the Colorado Ultraviolet Transit Experiment (CUTE) cubesat,” in *UV, X-Ray, and Gamma-Ray Space Instrumentation for Astronomy XXII*, O. H. Siegmund, Ed., **11821**, 1182117, International Society for Optics and Photonics, SPIE (2021).
- 20 J. Hennessy, A. D. Jewell, M. E. Hoenk, *et al.*, “Metal-dielectric filters for solar-blind silicon ultraviolet detectors,” *Appl. Opt.* **54**, 3507 (2015).
- 21 J. R. Lemen, A. M. Title, D. J. Akin, *et al.*, “The Atmospheric Imaging Assembly (AIA) on the Solar Dynamics Observatory (SDO),” *Sol. Phys.* **275**, 17–40 (2012).
- 22 E. N. Hertz, P. N. Cheimets, W. A. Podgorski, *et al.*, “Design, analysis, and performance verification of the interface region imaging spectrograph (IRIS) telescope primary mirror assembly,” in *Space Telescopes and Instrumentation 2012: Ultraviolet to Gamma Ray*, T. Takahashi, S. S. Murray, and J.-W. A. den Herder, Eds., *Society of Photo-Optical Instrumentation Engineers (SPIE) Conference Series* **8443**, 84433F (2012).
- 23 W. A. Podgorski, P. N. Cheimets, L. Golub, *et al.*, “Design, performance prediction, and measurements of the interface region imaging spectrograph (IRIS) telescope,” in *Space Telescopes and Instrumentation 2012: Ultraviolet to Gamma Ray*, T. Takahashi, S. S. Murray, and J.-W. A. den Herder, Eds., *Society of Photo-Optical Instrumentation Engineers (SPIE) Conference Series* **8443**, 84433D (2012).
- 24 W. A. Podgorski, D. Caldwell, K. McCracken, *et al.*, “Minimizing the mirror distortion for subarcsecond imaging in the Hi-C EUV telescope,” in *Advances in X-Ray/EUV Optics and Components VII*, S. Goto, C. Morawe, and A. M. Khounsary, Eds., *Society of Photo-Optical Instrumentation Engineers (SPIE) Conference Series* **8502**, 85020E (2012).
- 25 A. Slocum, “Kinematic couplings: A review of design principles and applications,” *International Journal of Machine Tools and Manufacture* **50**(4), 310–327 (2010). Design of Ultraprecision and Micro Machine Tools and their Key Enabling Technologies.
- 26 J. Anderson and I. R. King, “Toward High-Precision Astrometry with WFPC2. I. Deriving an Accurate Point-Spread Function,” *PASP* **112**, 1360–1382 (2000).
- 27 LUVVOIR Final Report *arXiv:1912.06219* (2019).
- 28 J. Rigby, M. Perrin, M. McElwain, *et al.*, “The Science Performance of JWST as Characterized in Commissioning,” *PASP* **135**, 048001 (2023).
- 29 J. V. Vallerga and O. H. W. Siegmund, “2K×2K resolution element photon counting MCP sensor with >200 kHz event rate capability,” *Nuclear Instruments and Methods in Physics Research A* **442**, 159–163 (2000).
- 30 J. V. Vallerga, J. B. McPhate, A. P. Martin, *et al.*, “HST-COS far-ultraviolet detector: final ground calibration,” in *UV/EUV and Visible Space Instrumentation for Astronomy and Solar Physics*, O. H. Siegmund, S. Fineschi, and M. A. Gummin, Eds., *Society of Photo-Optical Instrumentation Engineers (SPIE) Conference Series* **4498**, 141–151 (2001).
- 31 “Nasa sounding rockets user handbook.” <https://sites.wff.nasa.gov/code810/files/SRHB.pdf> (2023).

- 32 “Astrophysics biennial technology report.” https://apd440.gsfc.nasa.gov/images/tech/2022_ABTR.pdf (2022).
- 33 J. I. Larruquert, M. Vidal-Dasilva, S. García-Cortés, *et al.*, “Multilayer coatings for the far and extreme ultraviolet,” in *EUV and X-Ray Optics: Synergy between Laboratory and Space II*, R. Hudec and L. Pina, Eds., *Society of Photo-Optical Instrumentation Engineers (SPIE) Conference Series* **8076**, 80760D (2011).
- 34 J. I. Larruquert, P. López-Reyes, N. Gutiérrez-Luna, *et al.*, “Narrowband mirrors tuned at the desired far UV spectral lines,” in *Society of Photo-Optical Instrumentation Engineers (SPIE) Conference Series*, J.-W. A. den Herder, S. Nikzad, and K. Nakazawa, Eds., *Society of Photo-Optical Instrumentation Engineers (SPIE) Conference Series* **12181**, 121813J (2022).
- 35 K. France, K. Hoadley, B. T. Fleming, *et al.*, “The SLICE, CHESSE, and SISTINE Ultraviolet Spectrographs: Rocket-Borne Instrumentation Supporting Future Astrophysics Missions,” *Journal of Astronomical Instrumentation* **5**, 1640001 (2016).
- 36 D. L. Windt and W. Cash, “The soft X-ray/EUV calibration facility at the University of Colorado,” in *X-ray calibration: Techniques, sources, and detectors*, *Society of Photo-Optical Instrumentation Engineers (SPIE) Conference Series* **689**, 167–177 (1986).
- 37 E. Farr, N. Kruczek, K. France, *et al.*, “Lyman-ultraviolet imaging filter development for the FLUID rocket payload,” in *UV, X-Ray, and Gamma-Ray Space Instrumentation for Astronomy XXIII*, O. H. Siegmund and K. Hoadley, Eds., **12678**, 126780T, International Society for Optics and Photonics, SPIE (2023).
- 38 O. Siegmund, J. McPhate, J. Vallerga, *et al.*, “Development of planacon tubes with cross strip readouts and atomic layer mcps,” in *2020 IEEE Nuclear Science Symposium and Medical Imaging Conference (NSS/MIC)*, 1–6 (2020).
- 39 C. Ertley, O. Siegmund, T. Cremer, *et al.*, “Performance studies of atomic layer deposited microchannel plate electron multipliers,” *Nuclear Instruments and Methods in Physics Research A* **912**, 75–77 (2018).
- 40 C. Ertley, O. H. W. Siegmund, J. Schwarz, *et al.*, “Characterization of borosilicate microchannel plates functionalized by atomic layer deposition,” in *UV, X-Ray, and Gamma-Ray Space Instrumentation for Astronomy XIX*, O. H. Siegmund, Ed., SPIE (2015).
- 41 R. A. Hock, P. C. Chamberlin, T. N. Woods, *et al.*, “Extreme Ultraviolet Variability Experiment (EVE) Multiple EUV Grating Spectrographs (MEGS): Radiometric Calibrations and Results,” *Sol. Phys.* **275**, 145–178 (2012).
- 42 N. Nell, K. France, A. Harwit, *et al.*, “Characterization of an ultraviolet imaging detector with high event rate ROIC (HEROIC) readout,” in *High Energy, Optical, and Infrared Detectors for Astronomy VII*, A. D. Holland and J. Beletic, Eds., *Society of Photo-Optical Instrumentation Engineers (SPIE) Conference Series* **9915**, 99152L (2016).
- 43 P. López-Reyes, B. Perea-Abarca, C. Honrado-Benítez, *et al.*, “Optimization of the deposition parameters of MgF₂/LaF₃ narrowband reflective FUV multilayers,” *Optical Materials Express* **11**, 1678 (2021).
- 44 P. López-Reyes, C. Honrado-Benítez, N. Gutiérrez-Luna, *et al.*, “Far-UV reflectance and stress of narrowband AlF₃/LaF₃ multilayers,” *Optical Materials Express* **12**, 489 (2022).
- 45 R. G. Ohl, T. T. Saha, S. D. Friedman, *et al.*, “Imaging Performance of Telescope Mirrors for Far-Ultraviolet Astronomy,” *Appl. Opt.* **39**, 4513–4523 (2000).
- 46 W. H. Steel, “The autostigmatic microscope,” *Optics and Lasers in Engineering* **4**, 217–227 (1983).
- 47 W. P. Kuhn, “Design and performance of a new compact adaptable autostigmatic alignment tool,” in *Optical System Alignment, Tolerancing, and Verification X*, J. Sasián and R. N. Youngworth, Eds., *Society of Photo-Optical Instrumentation Engineers (SPIE) Conference Series* **9951**, 995109 (2016).
- 48 R. E. Parks and W. P. Kuhn, “Optical alignment using the Point Source Microscope,” in *Optomechanics 2005*, A. E. Hatheway, Ed., *Society of Photo-Optical Instrumentation Engineers (SPIE) Conference Series* **5877**, 102–116 (2005).
- 49 T. A. Cook, W. Cash, and J. C. Green, “Far ultraviolet spectrophotometry of BD +28 4211,” *Advances in Space Research* **11**, 29–32 (1991).
- 50 C. L. Smith, “Basic confocal microscopy,” *Current Protocols in Molecular Biology* **44**(1), 14.11.1–14.11.12 (1998).
- 51 M. D. Perrin, R. Soummer, E. M. Elliott, *et al.*, “Simulating point spread functions for the James Webb Space Telescope with WebbPSF,” in *Space Telescopes and Instrumentation 2012: Optical, Infrared, and Millimeter Wave*, M. C. Clampin, G. G. Fazio, H. A. MacEwen, *et al.*, Eds., *Society of Photo-Optical Instrumentation Engineers (SPIE) Conference Series* **8442**, 84423D (2012).